EXPERIMENTAL EVIDENCE FOR CHANGES OF THE VECTOR MESON PROPERTIES IN HEAVY-ION COLLISIONS[a]

Johann Peter Wurm
Max-Planck-Institut für Kernphysik
Saupfercheckweg 1, D-69117 Heidelberg, Germany
e-mail: jpw@fossy2.mpi-hd.mpg.de

The enhanced dilepton production observed by experiments at the CERN SPS is reviewed with emphasis on recent CERES Pb–Au data. The enhancement is strongest between the 2-pion threshold and the rho/omega resonance, and grows stronger than linear with centrality, which supports the expectation that pion annihilation of thermal origin is the dominant source. Theoretical calculations seem to require medium modifications as an essential ingredient to describe the low-mass dilepton excess by shape and magnitude, either by a dropping in-medium mass of the rho meson as a precursor of chiral symmetry restoration, or by collisional broadening. The medium modifications manifest in the invariant mass spectra appear to be strongly localized at transverse momentum below a few hundred MeV/c. This suggests an explanation why low-mass spectra measured by NA38/50 at larger p_t look so different.

1 Introduction

The ultimate goal of ultra-relativistic heavy-ion physics is the exploration of new states of matter that are believed to have existed until a few tens of microseconds after 'big bang' - and might be formed in the very hot and dense environment of a nuclear fireball in the laboratory. As well known, the field was stimulated by predictions of lattice QCD calculations that ordinary hadronic matter at high energy density undergoes a phase transition into a plasma of deconfined quarks and gluons (QGP). Impressive efforts have been made in preparing suitable conditions for quark matter to be formed in heavy-ion collisions, and for detection of characteristic signals. However, no signal could stabilize yet as positive evidence without being given alternative explanation in terms of a hadronic scenario [1].

Instead of searching for features indicating new states of matter, one might as well look out for changes of the 'known', especially if the phase transition should be soft [2]. Such an alternative approach to new vistas uses penetrating probes to explore hadrons inside the dense and hot environment for modified properties, unusual features or correlations that reflect proximity to the phase boundary. In fact, an analysis of abundance ratios of particles produced in

[a]Invited talk given at the ACTP Workshop on Hadron Properties in Medium, in Honor of Mannque Rho's 60th Birthday, Seoul, October 27-31, 1997

nucleus-nucleus collisions at the Brookhaven AGS and the CERN SPS indicates that the matter resided close to the phase boundary, even at freeze-out [3]. Apart from the potential to attack profound physics aspects, it is mandatory to investigate hadronic processes at highest densities and temperatures as they will entangle future data from experiments at RHIC and LHC.

The eminent physics issue is restoration of chiral symmetry. It is supposed to make its appearance already at some distance away from the phase boundary. This symmetry of quantum chromodynamics in the limit of vanishing quark masses is spontaneously broken in the complex QCD vacuum. The physical vacuum is a condensate of scalar quark-antiquark (and gluon) pairs that repels color electric fields to squeeze them into hadrons [4]. The energy gap characteristic of spontaneous breaking of chiral symmetry is of order 1 GeV. It separates pseudo-scalar π, η, and K mesons at the bottom, nearly massless Goldstone bosons, from vector mesons and nucleons which become massive. QCD lattice simulations suggest that chiral symmetry is approximately restored at a temperature of about 150 MeV. The reduction of the condensate with temperature can be visualized as being effected by the scalar quark density contained in thermal pions. Adding baryons to the vacuum, i.e. turning on a baryon chemical potential, is supposed to be an even stronger reagent for reducing the quark condensate. Thus, 'melting' of the condensate under conditions of finite temperature and/or baryon density is to affect the masses of light-quark hadrons, vector mesons in particular.

Vector mesons provide also the key to measurement of medium changes. As Pisarski foretold [5], the onset of critical behavior might be observable from prompt dilepton production in very hot fireballs by changes in the position and width of the ρ-meson peak. The isovector $\rho(770)$ meson, strongly coupled to the $\pi\pi$ channel, is a short-lived ($\tau=$ 1.3 fm/c) and major constituent of the pion-dominated hot hadron gas, and the binary reaction $\pi\pi \rightleftharpoons \rho$ proceeds both ways in chemical equilibrium [b]. Most rho mesons will decay inside the fireball into pions which interact many times and leave no measurable traces. Only a tiny fraction of about 1 in 10^4 rho's decay electro-magnetically into a lepton pair, $\rho(m^*) \to \gamma^*(m^*) \to \ell^+(p_+)\ell^-(p_-)$, and the mass m^* of the ρ at the instant of its decay is transported in the 4-momenta p_+, p_- of the electron or muon pair without distortion, to be measured in a pair spectrometer as the pair invariant mass $m^2 = (p_+ + p_-)^2 = m^{*2}$.

This elegant (highly simplified) view will be clouded, however, once vector mesons suffer strong collisional broadening in hot matter [6] and loose their visibility in mass spectra. Extraction of the mass, the pole position, then

[b] In partial chemical equilibrium with $\mu_\pi \neq 0$, vector mesons acquire chemical potentials $\mu_\rho = 2\ \mu_\pi$ from the binary reaction and $\mu_\omega = 3\ \mu_\pi$ from the ternary reaction.

becomes very model dependent, while on the theory side, the rho meson as a quasi-particle propagating in dense matter might no longer remain a useful concept. This speaks for the $\omega(783)$ meson with natural width $\Gamma_{\pi\pi\pi}= 8.4$ MeV/c^2, or $\tau= 23$ fm/c, as a suitable object for future precision studies of medium properties.

Gerry Brown and Mannque Rho proposed [7] the universal scaling idea in 1991 which states that the masses of all hadrons made of light quarks, save the Goldstone bosons, decrease in dense matter together with the chiral condensate,

$$\frac{m^*}{m} = \frac{\langle\psi\bar{\psi}\rangle^*}{\langle\psi\bar{\psi}\rangle}. \tag{1}$$

With Brown-Rho scaling vector meson masses go to zero in sufficiently hot and/or dense matter. It seems to be supported at low temperature by QCD sum rule analyses [8] and nuclear physics arguments [9]. Conversely, assuming vector meson dominance, an increasing $m_\rho(T)$ has also been predicted [10]. Symmetry arguments alone would only require that chiral partners (π, σ) and (ρ, a_1), etc. become degenerate without prescribing where and how the pole strengths will be located, as pointed out by Kapusta and Shuryak [11]. So Brown-Rho scaling is a highly non-trivial dynamical hypothesis rich in predictive power that one would like to convincingly identify , or disprove, in experiment.

Recent interest in the physics of dense hadron matter was stimulated by data from three CERN experiments. HELIOS/3 [12], CERES/NA45 [13] and NA38 [15] have observed significantly more dileptons in central collisions of 200 GeV/nucleon sulfur beams with heavy targets than one would expect from a mere superposition of proton-proton collisions. The CERES data were clearly suggestive of electron pair production by annihilation of pions in the dense and hot medium [16]. It was early suggested by Li, Ko and Brown [17] that a dropping of the in-medium ρ mass provides the missing strength at about two thirds of the free mass for a perfect description of the CERES data –while a variety of 'more conventional' approaches failed to do so. Those rival explanations invoke in-medium modifications due to hadronic collision processes that lead to a *broadening* [18], rather than a *shift* of the ρ spectral function. As we shall see below, present dilepton data are far from being sufficiently accurate to discard one or the other approach.

The study of hadronic phenomena close to the phase boundary has become a very lively field. The fundamental physics aspect of it, mass shifts that indicate vacuum changes in hadron matter due to restoration of chiral symmetry –if the ideas of Brown and Rho are correct– definitively adds a very special challenge. Aside from CERN experiments, it has inspired also activities to measure vector meson properties inside normal nuclei, like electro-production of vector mesons [19], threshold photo-production of rho in ^{3}He [20], and recoilless ω production in nuclei [21].

After some introductory notes on dilepton production in hadron and nucleus-nucleus collisions, in general, and on the experiments at the CERN SPS, in particular, I review the enhanced production observed in the CERN data with the sulfur beam in the low- and intermediate-mass region, and give a layman's reminder of previous theoretical work. Much what I have to say here was said before in reviews by my colleagues A. Drees [22] and I. Tserruya [23] which cover also the real photon sector which still holds promise for excitement in future. I will proceed to present the recently completed analysis of the CERES 1995 data with the Pb beam. After a critical view into signal recovery and its stability, I will discuss the novel features of these data, the dependencies on centrality and transverse momentum, and look out for the present status of understanding and the next steps to go in experiment.

2 Lepton pairs from hadronic and nuclear collisions

2.1 Overview: dileptons from hadron collisions

Fig. 1 displays a schematic mass spectrum indicating the major dilepton sources in hadron-hadron collisions. Vector meson resonance peaks are the most prominent, identifiable features; we will return to their discussion below. Dilepton emission from hard perturbative QCD processes is characteristic of the high-mass region (HMR). The Drell-Yan process (D-Y) is due to quark-antiquark annihilation

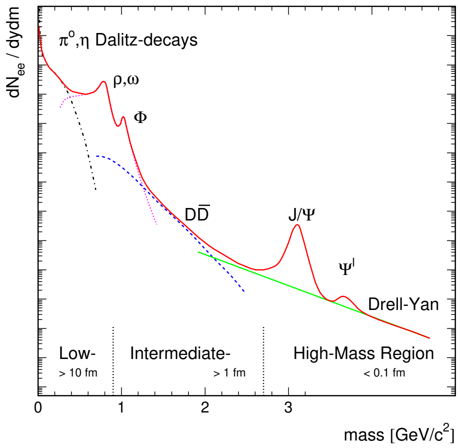

Figure 1: Schematic mass spectrum of dileptons from hadron collisions

$$q\bar{q} \rightarrow \gamma^* \rightarrow \ell^+\ell^- \tag{2}$$

and produces a hard continuum with a power-law falloff. K factors around 2 are needed to bring up the commonly used leading-order calculations, for instance with the PYTHIA code up, to match experimental cross sections. D-Y serves as a reference cross section above 1.5 GeV/c^2. Lower masses derive from progressively lower fractions x of the nucleon momentum in the generating parton distributions which are less well known [24].

Associated $D\bar{D}$ production is the main process underlying the continuum in the intermediate mass region (IMR). The open charm mesons originate from $c\bar{c}$ pairs formed in primary hard collisions like gluon fusion which subsequently bind with light quarks. The simultaneous but uncorrelated semileptonic decays into lepton and anti-lepton are not easily distinguished from genuine lepton pairs and might be a formidable source of combinatorial background at LHC [25]. As shown recently [26], open charm production is well reproduced for p–A collisions by the PYTHIA Monte-Carlo code [27].

The LMR is the regime of soft processes. The peak structure is due to the direct decays of ρ and ω and remains usually unresolved. Dilepton continua originate from Dalitz decays of neutral mesons, $\pi^\circ \rightarrow e^+e^-\gamma$, $\eta, \eta\prime \rightarrow \ell^+\ell^-\gamma$, and $\omega \rightarrow \ell^+\ell^-\pi^\circ$. The yield rises steeply towards low masses and low transverse momentum $p_\perp$. For most of our purposes, dileptons from decays of neutral mesons are merely physics background with a tendency to cover prompt dileptons of low mass and p_t we might be looking for. However, they also provide a suitable *reference* for dilepton production in nucleus-nucleus collisions when scaled with charged-particle density. The simulation of this source of dileptons is commonly referred to as the 'cocktail of hadronic sources' somewhat obscuring the fact that dileptons from hadro-chemical reactions, like $\pi\pi$ annihilation, etc. are *not* included.

2.2 Dileptons from nucleus-nucleus collisions

J/Ψ suppression exhibited by the new NA50 dimuon data for central lead-lead collisions [28] is surely the most interesting current physics topic of dilepton production in the HMR. Whether it signals 'anomalous' extinction in de-confined matter, as proposed originally by Matsui and Satz [29], see also ref. [30], or can be explained by hadronic response, is still in dispute; no doubt, it indicates that very hot and dense matter has been created! We remark that the long-lived J/Ψ does not convey its in-medium properties since it decays in vacuum.

J/Ψ suppression is a reminder of the importance of the medium even in hard processes. Besides propagation, the production cross section itself is affected via modified parton distributions. Secondary D-Y in heavy-ion collisions at SPS energies has been analyzed by ref. [31] with URQMD [32] to find substantial contributions to the IMR by replacing sea $\bar{q}$ in primary nucleon-nucleon collisions by hard $\bar{q}$'s in produced mesons and anti-baryons [c]. Enhancement of open charm production in nucleus-nucleus collisions is still a widely open issue; positive indications from NA38/50 will be discussed below.

Let us turn to thermal pair production. The large and long lived aggregate of interacting particles forming a dense and continuous medium, the 'fireball' or 'fire-cylinder', distinguishes nucleus-nucleus collisions from hadron collisions, at least conceptually. It is created by stopping followed by local thermalization and resides in the central rapidity region. We like to study this object of high energy density with the penetrating probe of dileptons.

Thermal dileptons are radiated in the course of hadro-chemical reactions (or secondary processes) directly as in annihilation processes in dense hadron matter, or by decays of short-lived hadronic reaction products. We add the Landau–Pomeranchuk effect for bremsstrahlung [34] from locally thermalized stages. Thermal dileptons produced in the plasma phase by $q\bar{q}$ annihilation and other QCD processes involving gluons are expected to be dominant in the HMR, maybe in the IMR, depending on initial energy density; considered long ago as QGP signature [35,36], they have not yet been identified. Thermal dilepton production in the IMR from secondary processes has been considered only very recently [37,38].

Two-pion annihilation is the dominant thermal process in the hadron gas phase that produces low-mass dileptons [39] and was considered already in context of early DLS data [40]. The annihilation cross section is that for point-like pions multiplied by the square of the electro-magnetic form factor of the pion in the time-like region,

$$\sigma_{ll}(M) = \frac{4\pi\alpha^2}{3M^2}\sqrt{1-\frac{4m_\pi^2}{M^2}} \mid F_\pi(M) \mid^2, \tag{3}$$

and it has been measured via the reverse reaction $e^+e^- \rightarrow \pi^+\pi^-$ to great accuracy as a function of $s = M^2$ in collider experiments [41]. The form factor is dominated by the rho meson pole, and approximating the more precise Gounaris-Sakurai parametrization by a Breit-Wigner form and also neglecting subtleties in shape including the ρ/ω mixing [42],

$$\mid F_\pi(M) \mid^2 = \frac{m_\rho^4}{(M^2-m_\rho^2)^2 + m_\rho^2\Gamma_\rho^2}. \tag{4}$$

[c] Concerning open charm, some optimism that thermal pairs might be not entirely hidden in background from $D\bar{D}$ pseudo dileptons derives from intra-nuclear absorption of charmed quarks [33].

The annihilation rate in the hot hadron gas derives from thermal average over the momentum distributions of the pions. Any appreciable shift in mass or change in the width of the rho, i.e. a change in the real or imaginary parts of the in-medium spectral function, will modify the invariant mass spectrum of dileptons [43]. Data will be compared to these calculations in sect. 4 and 5. For prime reference, the paper of Li et al. [38] in these proceedings should be consulted.

Medium modifications of the older kind were connected to hadronic rescattering processes. An example is the softening of the pion dispersion relations due to the attractive p-wave interaction between pions and nucleons in dense hot matter which *increases* the number of pions and hence the annihilation rate, as described by Gale and Kapusta [39]. The resulting dilepton enhancement [d], however, is negligibly small [45], see also below.

The rho meson is surrounded by a cloud of pions that couple strongly to nucleons and thermally excited Δ's and so get mixed with ΔN^{-1} excitations. This causes a *broadening* of the rho spectral spectral function in hot baryonic matter. As with the dropping mass, dilepton production is affected via the modified form factor of the pion. This branch of thought is rooted in the early work by Herrmann, Friman, and Nörenberg [46], Asakawa, Ko et al. [47], and Chanfray and Schuck [48]. It was developed further by inclusion of rho-like particle-hole resonances, like $N^*(1720)N^{-1}$ and $\Delta(1905)N^{-1}$, which are strongly excited in p-wave ρ-N and ρ-Δ scattering in baryonic matter at finite temperature, as proposed by Friman and Pirner [49]. Rho meson propagation in matter has been systematically studied and quantitatively applied to the enhancement of low mass dilepton production by Chanfray, Rapp and Wambach [18,50] and Steele, Yamagishi and Zahed [51], see sec. 4. For the true story as well as the latest developments I refer to the contributions of B. Friman [52] and I. Zahed [53].

At least superficially, the interaction-induced modifications seem rather disconnected from chiral symmetry restoration. The mixing between vector and axial-vector currents as the leading temperature effect in approaching restoration of chiral symmetry has the tendency to *reduce* pion annihilation on-resonance, as has recently been remarked by Song and Koch [45], quoting Dey, Eletsky, Ioffe [54] that up to terms of order T^2 there is only mixing, but no mass shift.

After sketching some of the dilepton production *rates* important in nucleus-nucleus collisions, the second ingredient to any calculation of dilepton data should not go unmentioned: the *evolution* of the collision system in which these processes take place. Dileptons originate from all stages and add up

[d] the prediction of a peak in the dilepton yield at m= $2m_\pi$ was disproved later [44].

cumulatively [55]. The space-time integral over the production rate involves the full reaction dynamics and depends on initial conditions, on the speed of thermalization, on whether or not there is a phase transition and which type of, on the equation(s) of state which define the cooling curve, the lifetime of the system and the expansion dynamics. The evolution is usually modeled in relativistic hydrodynamics, with initial conditions given by cascade event generators such as Fritjof, Venus or RQMD.

The large number of theoretical inputs necessary to model dilepton emission in a nucleus-nucleus collision is felt somewhat off balance in view of the limited amount of relevant data. One might expect that model parameters can be chosen at considerable liberty, since hadronic data hardly constrain the dynamics of the early collision phases [69]. The experimental handle to unravel different dilepton continua is not very powerful and in view of the small cross sections, expectations in this direction can only be modest. Still, present-day experimental limitations in acceptances of all sorts are not installed by law of nature, and better ways will be found to isolate certain processes and differentiate between theoretical models. It is a big challenge towards this objective to exploit more of the seven physics variables available [e], a small progress in this direction is presented with the new CERES data below.

Despite these limitations, there is a very useful criterion for thermal processes based on the fact that their rate is proportional to the square of the local pion density, like for any other binary reaction between primary hadrons [f]. Under certain simplifying assumptions, the thermal yield will scale as the *square* of the charged-particle density dN_{ch}/dy [39], in contrast to decays of primary hadrons which scale *linearly* with dN_{ch}/dy. This rule is not strict; but observation of any stronger-than-linear dependence of the dilepton yield on charged multiplicity is sufficient to safely infer thermal radiation.

3 Dilepton Experiments at the CERN SPS

After the Dilepton Spectrometer Collaboration (DLS) stopped to take data at the Bevalac at 1 AGeV/c^2 [40,56] in 1993, all experiments on dilepton production in proton-nucleus and nucleus-nucleus collisions have been performed at the CERN SPS. The NA34/HELIOS program is discontinued. HELIOS/1 measured electron and muon pairs in p–Be collisions at 450 GeV/c beam momentum. Two dimuon experiments extended the range of invariant masses up to and beyond the J/Ψ, HELIOS/3 in p–W and S–W collisions, and NA38 in

[e] counting e.g. y, centrality (for N_{ch} or E_T), m, p_t (or other combinations), $\sqrt{s}$, choice of the colliding system A–B, and some lepton emission angle in the γ^* rest frame.

[f] for a ternary reaction like $\pi\pi\pi \rightarrow \omega$, it would scale with the cube.

Table 1: Dilepton experiments at CERN SPS using p beams of 200 or 450 GeV, S beams of 200 AGeV, and Pb beams of 158 AGeV.

Experiment	Pairs	System	y_{lab}	m_T(GeV/c)	Mass(GeV/c^2)
HELIOS/1}	$\mu^+\mu^-$, e^+e^-	p–Be	≥ 3.5	$\geq$0.5	0.3–1.5
HELIOS/3}	$\mu^+\mu^-$	p,O,S–W	3.9–5.8	$\geq$0.5	0.3–4.0
CERES	e^+e^-	p–Be, p–Au	2.1–2.65	$p_t \geq 0$	0.2–1.5
		S–Au			
		Pb–Au			
NA38}	$\mu^+\mu^-$	p–A, S–U	3.0–4.0	$\geq$1.0	0.3–4
NA50	$\mu^+\mu^-$	Pb–Pb	2.8-4.0	$\geq$1.5	1.5–7.0

p-U and S-U collisions together with its successor NA50 in Pb-Pb collisions. NA45/CERES[g] is the only electron-pair spectrometer in operation, it is devoted to the low-mass region. HELIOS/3 and NA38/50 are high-luminosity experiments that detect muon pairs in large-size chambers behind long absorbers that filter out all primary hadrons, and are positioned at forward pseudo-rapidity[h].

Table 1 compares the acceptances. NA38/50 for its purpose to measure massive pairs, has an acceptance in transverse mass $m_T = \sqrt{p_T^2 + m^2}$ of about 1 GeV/c^2 [i], very suitable for hard processes. Around and above the ϕ all p_t are accepted. However, a severe p_t threshold is introduced for low-mass pairs of 0.8 GeV/c at m= 0.5 GeV/c^2, and still of 0.6 GeV/c at the ρ/ω mass! The m_T acceptance of HELIOS/3 is more soft[j] and there is no p_t cut for m$\geq$0.5 GeV/c^2.

The CERES experiment is in many ways diametrically different (see sec. 5). Among its advantages is its acceptance close to mid-rapidity and the absence of a low-p_t cut-off. It suffers, however, from three orders of magnitude lower luminosity. That effectively limits the range in invariant mass to around 1.5 GeV/c^2.

[g]for CErenkov Ring Electron Spectrometer

[h]For details on detectors see ref.[91] for HELIOS/3, ref.[92] for NA38, ref.[93] for NA50, and ref.[94] for CERES.

[i]It is given by $m_T \geq 0.9 + 2\,(y_{lab} - 3.55)^2$ (GeV/c), with an average of 1.1 GeV/c over the acceptance.

[j]It is given by $m_T \geq \sqrt{4\,m_\mu^2 + 225/\cosh^2(y_{lab})}$ (GeV/c), with an average of 0.5 GeV/c over the acceptance.

4 Dilepton Results from p and S Beams

4.1 The reference

In fig. 2, the CERES e^+e^- invariant mass spectra for 450 GeV p–Be and p–Au collisions, and 200 AGeV S–Au collisions are compared to the expected contributions from hadron decays. This 'cocktail' of e^+e^- pairs from neutral meson decays is simulated by scaling up p–p data with charged-particle density, after minor adjustments in p_t and y distributions to A–A conditions, and application of experimental acceptance cuts and filter conditions as used in the off-line analysis. Our knowledge is based on a systematic study of the production and electromagnetic decay of neutral mesons, supplemented by exclusive measurements of the η-Dalitz decay contribution to the e^+e^- pair spectrum by the CERES/TAPS Collaboration [57]. Evidently, the hadronic sources account for the measured dilepton yield in p–Be collisions very well which confirms the earlier conclusion of HELIOS/1 with significantly reduced systematic uncertainties. The methods of defining the p–p reference to be used for dilepton production in nucleus-nucleus collisions and their uncertainties have been elaborated recently for hadron decays [57,22] and hard or semi-hard processes [58]. Small contributions from pion annihilation and bremsstrahlung as found by Cassing et al., see refs.[65,73] in p–Be, p–W and stronger in p–Au, where a shifting rho mass starts to be indicated in the calculations of Li et al. [66], are not in contradiction at present error limits with the observation that the hadronic cocktail of neutral meson decay sources alone describes the p–A data so well. The contribution from charm decays have been extrapolated to the LMR [26].

4.2 Enhancement of Dilepton Yields

In contrast, the pair yield measured in the S–Au system exceeds significantly the expectation from p–p collisions over the entire spectrum, except for the first three data points that are well described by π°-Dalitz decay. Note that very soft pairs are strongly reduced in comparison to p–Be and p–Au due to a harder cut on p_t of accepted electron tracks of 200 MeV/c, instead of 50 MeV/c. Integrating over the mass region from 0.2 to 1.5 GeV/c^2, the dilepton yield in S–Au is enhanced by a factor $5.0 \pm 0.7(stat.) \pm 2.0(syst.)$. At and below the ρ/ω, the shape of the spectrum is changed in a most conspicuous way: the local minimum around 0.6 GeV/c^2 is not only filled up entirely, but the surplus rises to a flat maximum around 0.4 GeV/c^2 –about halfway between the two-pion threshold and ρ/ω– masking the resonance by the plateau. In p–Be and p–Au, despite the poor 1993 mass resolution of $\sigma_m/m \approx 11\%$, ρ/ω is seen as

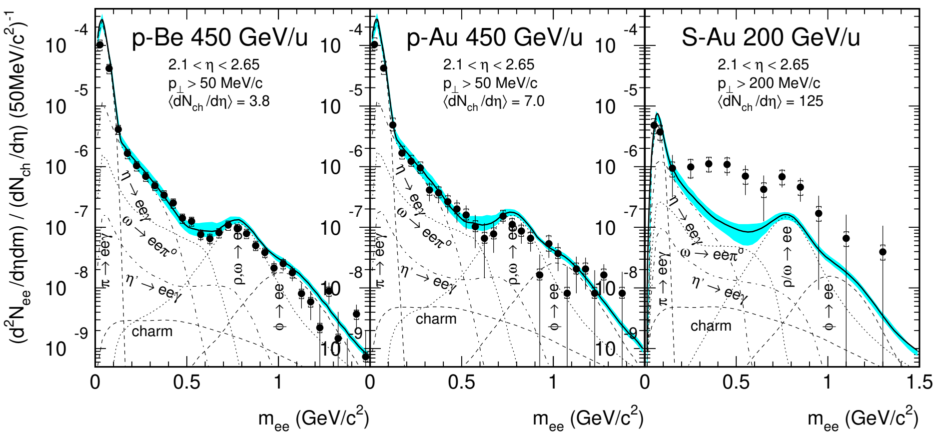

Figure 2: Inclusive e^+e^- mass spectra for p–Be, p–Au and S–Au measured by CERES. The yield per collision $d^2N_{ee}/d\eta dm$ is normalized to the observed charged-particle density. Statistical errors (bars) and systematic errors (brackets) are marked on the data points. The lines denote the generator simulated decays from neutral mesons as labeled. The grey band indicates the systematic uncertainties of the summed contributions.

a prominent peak.

Dilepton production in S–Au collisions is evidently not described well by merely adding the sources from independent p–p collisions. This need not signal 'new physics' to us but should be registered as the observation of thermal dilepton emission from the hot hadron gas. The prime candidate reaction is pion annihilation with a threshold at $m_{ee} = 2m_\pi$ which was discussed in Sect. 2.

An enhanced dilepton production was also observed by the HELIOS/3 Collaboration [12] in S–W collisions compared to p–W. The enhancement extends over the entire mass range up to J/Ψ, where the illustrious suppression is visible in fig. 3.

In the LMR, we have deduced from HELIOS/3 data plots at $y \approx 4.2$ an enhancement factor of $data(\text{S-W})/data(\text{p-W}) = 1.65 \pm 0.15(stat.)$ for $0.2 \leq m \leq 1.5$ GeV/c^2. Systematic errors are unknown. We note that particle densities in central collisions are smaller by a factor of 2–3 in the more forward acceptance of HELIOS/3 than in the CERES acceptance. It has been suggested [16,22] that the different magnitudes of the low-mass enhancement seen by CERES and HELIOS/3 would be compatible with an identical dilepton source, if the yield would scale as the square of the charged particle multiplicity. We shall revisit this topic with the Pb–Au for data in sect. 5.

To quantify the enhancement of the intermediate-mass continuum appar-

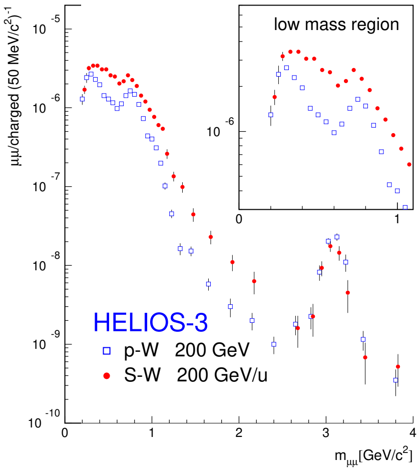

Figure 3: Invariant-mass spectra of muon pairs measured by HELIOS/3 in p–W and in central S–W interactions in log scale. Insert displays low-mass region. The yields are normalized to the charged-particle multiplicity in the spectrometer acceptance, ref. [12].

ently seen in fig. 3, the reference yield for S–W was obtained from p–p data by extrapolating three sources: the high-mass tails of light vector mesons, pairs from semi-leptonic decays of $D\bar{D}$, and D-Y [k]. In the interval $1.5 \leq m \leq 2.5$ GeV/c^2, the HELIOS/3 ratio $data$(S-W)/$prediction$(S-W)$\approx$ 2.5; for p–W, the ratio is 1 within errors.

The intermediate-mass excess in central S–U collisions was reported by NA38 already at QM'93 [15]. With linear extrapolation of D-Y and charm from p–W, the enhancement in $1.5 \leq$ m ≤ 2.0 GeV/c^2 is about 1.5 and in shape consistent with enhanced charm production. NA50 reported for Pb–Pb collisions an enhancement in $1.5 \leq$ m ≤ 2.5 Gev/c^2 close to 2.0, without significant centrality dependence [59,22]. For a description of this 'excess' in terms of secondary reactions involving a_1 vector mesons is given in [38].

More recent analyses of p and sulphur dimuon data obtained from the NA38/50 'low-mass setup' [60] are shown in fig. 4. The yield declines abruptly already at m$\approx$ 0.5 GeV/c^2 where the effective p_t cut is up to about 0.8 GeV/c, still much harder than in HELIOS/3 [l]. The p–U data are found plainly off the reference given by the hadronic cocktail plus open charm for masses below 0.7 GeV/c^2. Once D-Y is extrapolated with PYTHIA from above J/Ψ down to

[k] the hard processes were linearly scaled in mass numbers [14], D-Y without nuclear modifications on quark distributions

[l] the NA50-Up configuration is currently under development to improve on low-p_t acceptance down to ρ/ω [61].

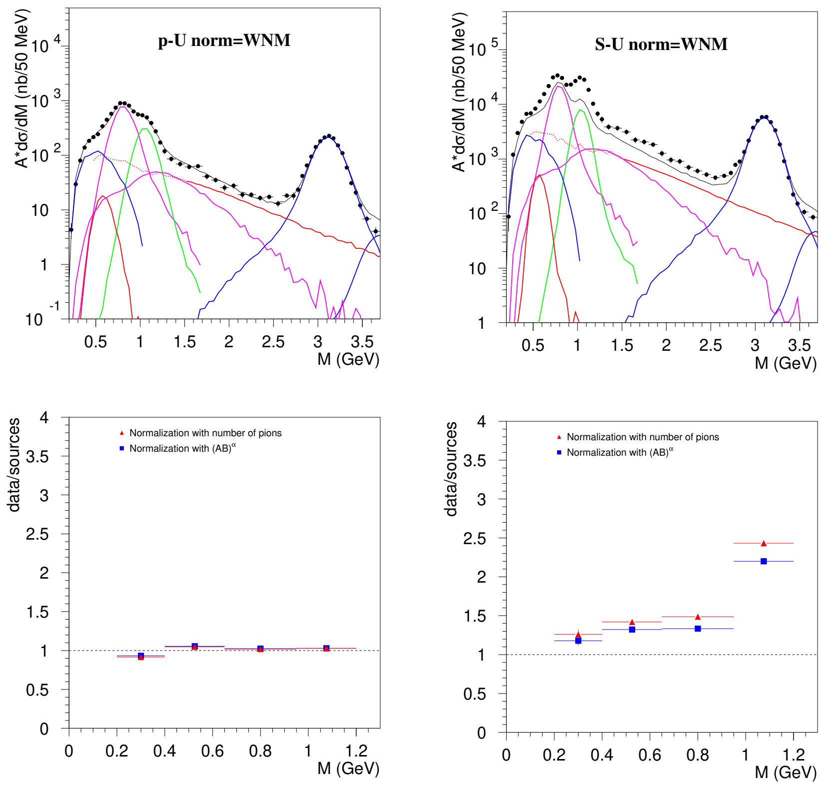

Figure 4: Mass spectra of muon pairs (upper row) for p–U data (left column) and S–U data (right column) of NA38 from ref.[60]. Inscribed lines are the expected contributions from the hadronic cocktail normalized to the number of 'wounded nucleons'. The two lines extending to high masses are D-Y and the softer open charm. *Data/Sources* ratio (lower row). Note that D-Y has been extended using (PYTHIA) down to 0.5 GeV/c^2.

0.5 GeV/c^2 (instead only to, say, 1.5 GeV/c^2), the good agreement shown in fig. 4 is obtained. That primary D-Y works still at 0.5 GeV/c^2 is astonishing. So some care might be advised on dealing with the low-mass excess in S–U reported by NA38/50[60] of approximately 25% to 30% around m$=$ 0.5 GeV/c^2 and in the ρ/ω mass region. Both dimuon experiments see an enhancement of $\phi/(\rho+\omega)$ ratio in S–induced compared to p–induced collisions[62,91].

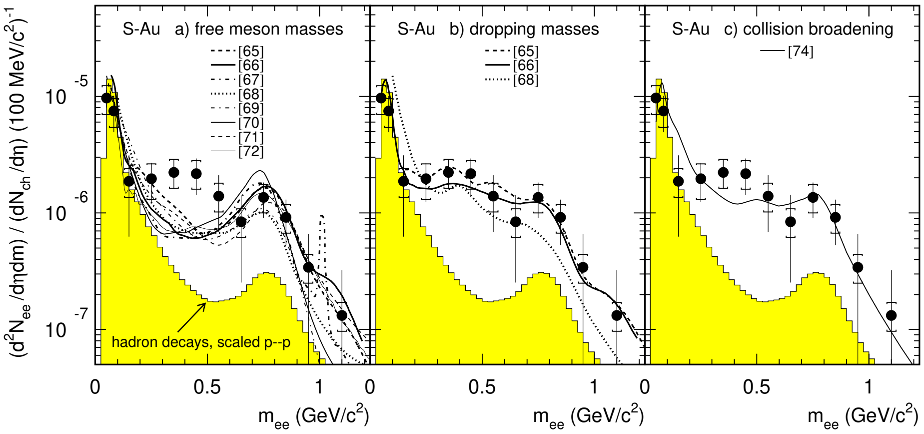

Figure 5: Calculated e^+e^- mass spectra with experimental acceptance cuts compared to CERES 200 AGeV/c S–Au data with statistical and systematic errors (brackets) and hadronic cocktail. A variety of calculations (refs. given in parentheses) using free meson masses are shown in the left panel, those with reduced in-medium masses in the center, and the unshifted but broadened rho-meson approach in the right panel; see text. Figure adopted from ref.[22].

4.3 Dilepton Enhancement: Model Calculations

The broad attack on the data sets of CERES and HELIOS/3 by many theorists has confirmed the expectation that the excess dileptons at and below the rho are closely related to pion annihilation of thermal origin, and other binary reactions involving vector mesons. The exciting news is that medium modifications of vector meson properties or their propagation are *essential* to describe the data. Figs. 5 and 6 give a compact reminder of the early theoretical calculations of refs.[65−74] for the CERES and HELIOS/3 sulfur data, respectively, incorporating experimental acceptance and filter conditions.

An overlay of calculations conventional in the sense that vector mesons keep their free space masses are displayed in the left panels of both figures[m]. We notice, that all spectra lie in a very narrow band and are in striking disagreement with data. In the mass region between $m \approx 2m_\pi$ and $m_{\rho/\omega}$ where the enhancement is largest, all calculations underpredict the data significantly, while at the rho/omega position they tend to overshoot; this applies to CERES and HELIOS/3 data as well. Pion annihilation is indispensable in all calculations in raising the yield above the hadronic cocktail m$\geq$ 200 MeV/c^2, but

[m] Some authors employ various scenarios that fall under more than one of our categories.

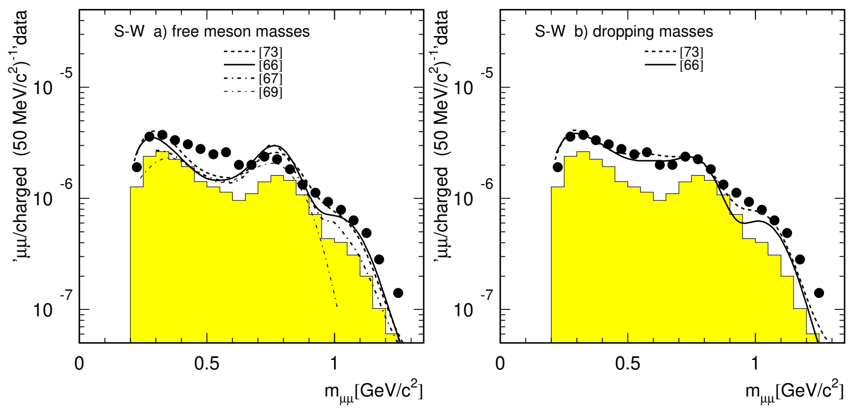

Figure 6: Calculated e^+e^- mass spectra with experimental acceptance cuts compared to HELIOS/3 200 AGeV/c S–W data and hadronic cocktail. Calculations using free meson masses are shown in the left panel, those with reduced in-medium masses at the right (refs. given in parentheses). Figure adopted from ref. [22].

insufficient to account for the excess around 400 MeV/c^2. This applies to calculations with the Hadron-String Dynamics model[63] of Cassing et al.[65,73] as to the relativistic fire-cylinder model of Li et al.[66], to the hydrodynamic models of Srivastava et al. [67] allowing for a first order phase transition, and of Hung and Shuryak [68]; to the hadronic transport calculation of Koch and Song [69] which does not invoke chemical equilibrium and incorporates modifications of the pion dispersion relations as mentioned before; to related approaches by Baier, Dirks, Redlich [70] and Murray, Bauer and Haglin [71] which take $\pi\rho$ scattering into account, and to the calculation of Winckelmann et al. [72] using UQMD, the Frankfurt non-equilibrium transport model: indeed an astounding degree of convergence, but away from the data!

In contrast, the falling meson-mass calculations look tailor-made, so well do they fit the invariant mass-spectra of CERES and HELIOS/3, as can be seen in the center panel of fig. 5 and the right panel of fig. 6. The downward shift of the rho mass creates extra yield by pion annihilation where the data show the strongest enhancement, and reduces the yield at the rho/omega peak accordingly. Let us take a somewhat closer look at some approaches using dropping masses to describe CERES and HELIOS/3 data.

The approach of Li, Ko, Brown[66] starts from a densely populated fire cylinder with initial abundances of mesons and baryons inserted from RQMD[32] calculations which then is let to expand in a relativistic transport model. Hadron masses are modified in response of their non-strange quark constituents to the

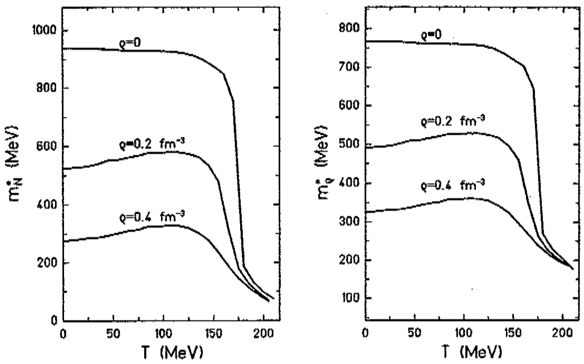

Figure 7: In-medium mass of nucleon (left) and ρ meson (right) as a function of temperature at several baryon densities, from ref.[66]. Densities correspond to 0, 1.25, and 2.5 times normal nuclear matter density.

scalar and vector mean fields that in turn are generated self-consistently at given baryon density and temperature[38]. Fig. 7 displays the falling of the nucleon and the rho-meson masses under the combined action of nuclear density and temperature. With starting conditions for the fire-cylinder expansion at T= 165 MeV, and $\rho_B \approx 0.4\,\mathrm{fm}^{-3} \approx 2.5\,\rho_\circ$, the rho mass drops to 270 MeV/c^2. The initial pion abundance of 0.45 fm^{-3} necessary to account for the observed pion rapidity spectra in the free-mass scenario decreases with falling masses to one half this value so that a large non-equilibrium pion chemical potential is no more required.

Cassing et al.[65,73] assume the QCD inspired version of falling vector meson masses[8],

$$m_\rho^* \approx m_\rho(1 - 0.18\rho_B/\rho_\circ) \qquad (5)$$

and obtain very similar results for similar starting conditions.

In their 'non-conventional' option in which chiral symmetry is assumed to be restored in the hot medium, Hung and Shuryak[68] let the masses of the vector mesons $\rho(770)$ and $a_1(1260)$ become equal (see previous introductory remarks), but for an empirical approach do not care to fix the final value, not even the direction of change. The curve in Fig. 5 corresponds to their case (D),$m_\rho^* = m_{a1}^* \approx 0.4\ m_\rho^\circ \approx 310$ MeV/c^2, which provides the best recipe to satisfy the data, and is remarkably close to the outcome of ref.[66], not inconsistent with Brown-Rho scaling because it seems unlikely that full restoration is achieved over the full lifetime of the fireball[n]. In-medium reduced rho mass was also

[n] At partial restoration, the Weinberg sum-rule relation $m_{a1} = \sqrt{2}m_\rho$ adopted by Li-Ko-Brown, if still valid, seems to be in conflict with the Hung-Shuryak scenario.

successfully employed by ref. [64], but their calculation is not shown.

The result of Rapp, Chanfray, Wambach [74] shown in the right panel of fig. 5 is obtained from the in-medium rho spectral function that acquires considerable broadening due to rescattering of the rho, as sketched in the introduction. The rho-like particle-hole excitations N(1790)N^{-1} and $\Delta(1905)N^{-1}$ deplete the rho peak and shift the strength downward, leading to an enhancement by a factor of 3 around m= 0.5 GeV/c^2 . In a recent extension of this work by Cassing, Bratkovskaya, Rapp and Wambach [75] the simultaneous description of both the CERES S–Au and the HELIOS/3 S–W data (not shown in fig. 6) in the spectral function approach (without falling masses) is quite good, also for Pb–Au data, see below.

5 The CERES 1995 Pb–Au data

5.1 CERES 1995

The first physics sample with the 160 AGeV/c Pb beam was taken in 1995 and consisted of 10 million triggered events. Some of the most physics relevant aspects of the instrumentation and the analysis I will report here before presenting the final results [76,77,78].

The CERES scheme to detect electron pairs in a large background of hadrons is to let them pass freely, together with photons from $\pi^\circ \rightarrow \gamma\gamma$ and other hadron decays, rather than absorb them [o]. This is achieved fairly successfully with two Ring Imaging Cerenkov (RICH) detectors operating at sufficiently high threshold, γ_{thr} = 32, to let all but a small percentage fraction of charged pions go undetected, and rigorously minimizing material within the acceptance. The RICH acceptance $2.0 \leq \eta \leq 2.65$ covers the central region. Full azimuthal symmetry warrants pair acceptance down to p_t=0.

The Pb-beam experiments are performed with external tracking, using a doublet of silicon drift detectors in front of RICH-1 and a large pad chamber downstream of RICH-2 which proved necessary to cope with the much larger background compared to S–Au or p–Be [79,80].

Events are triggered by beam particles which enter the target and disintegrate [p], conditional to a sufficiently large response by a scintillator ring at $2.9 \leq \eta \leq 4.7$ positioned 5 m downstream. This centrality trigger selects about 35% of σ_{geo}. Event selection by charged-particle multiplicity is done in the off-line analysis using the precise silicon-drift detector data.

[o] exception to this is a W barrel shielding the UV detectors from low-energy particles going backward from the target.
[p] Pb ions leaving the target intact are vetoed by an air Cerenkov counter.

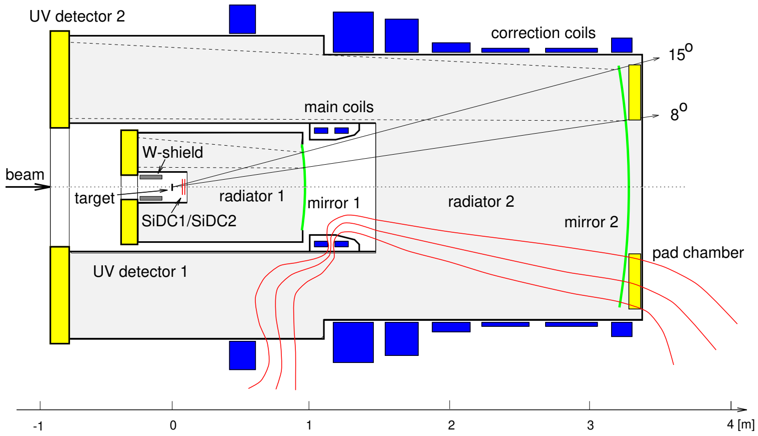

Figure 8: The CERES spectrometer consists of two axially symmetric Ring Imaging Cerenkov detectors [94]. The radiators are placed one behind the other and are separated by a compact magnetic field that deflects particle trajectories in azimuth for momentum analysis. There is no deflection within the radiators, B$\approx$ 0 in the first, and $\vec{B} \parallel \vec{p}$ in the second radiator, to obtain sharp ring images and recognize close pairs in the first RICH.

5.2 Tracking and momentum resolution

In analysis of the 1995 data, the new tracking capability was fully exploited. Inter-calibration between detectors was greatly improved by using high-momentum pion tracks [81]. The first step in the off-line track reconstruction is to find the interaction vertex using more than hundred charged-particle tracks traversing the doublet of silicon-drift detectors. At the end of the procedure, final electron tracks are identified by rings of asymptotic radius in both RICHes, with three space points before RICH-1, one space point behind RICH-2, and the two angles from the RICHes. The momentum is determined combining all track elements weighted according to detector resolution and multiple scattering. As a result, the momentum resolution is improved significantly, and a better mass resolution of $\sigma_m/m \approx 8\%$ at the ρ/ω resonance is obtained, compared to about 11% before.

Moreover, the fine tracking quality assures that even at high N_{ch} fake tracks are on a few percent level. This result relies on a number of carefully chosen and tested 'quality' cuts. The track finding efficiency was slightly above 0.5, corresponding to about 25% pair reconstruction efficiency. For details refs. [77,78] should be consulted.

By far the largest number of electron tracks belongs to e^+e^- pairs from photon conversions on material within the acceptance, and from π°-Dalitz decays. Both are called 'close pairs' because of small opening angles and have low invariant mass; let me focus on the Dalitz pairs. About 90% of all pairs with opening angles smaller than 50 mrad and invariant masses below 150 MeV/c^2 result from Dalitz decays. As a measure against combinatorial background, the physics pair sample is restricted to m$\geq$ 200 MeV/c^2. A Dalitz pair sample with m$\leq$ 200 MeV/c^2 is also collected. Despite being unavoidable physics

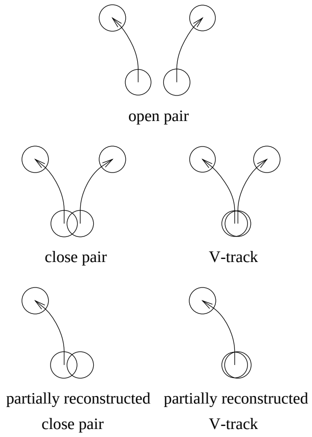

Figure 9: Sketch of e^+e^- event patterns depicting Cerenkov rings in RICH-1 below those in RICH-2 and arcs to symbolize opposite ϕ deflection of e^+ and e^-. Asymptotic ring diameters are 60 mrad. Top: open signal pair originating from ρ decay. Center: 'Close' pairs, a Dalitz pair (left) and conversion pair (right) not resolved in RICH-1 (V track). Bottom: partially reconstructed tracks, the main source of combinatorial pair background.

background, this well-known and strong source of electron pairs has been very suitable to assess pair reconstruction efficiency *vs* N_{ch}. The decay electrons [q] have a small opening angle θ_{ee} [r] and are soft: only 4% of those entering CERES acceptance will survive after requiring for each electron $p_t^e \geq 200$ MeV/c. Applying cuts on p_t^e of the electrons, and on the pair-opening angle, $\theta_{ee} \geq 35$ mrad, most Dalitz decays are separated and removed before tracks are combined to the 'open' signal pairs. Recognition of close pairs is accomplished in the silicon-drift telescope by two-fold double-dE/dx signals, or closely spaced

[q] stands for e^+ or e^-

[r] $\theta_{ee} \approx 30$ and 12 mrad(rms), for $p_t^e \geq 0$ and 200 MeV/c, respectively.

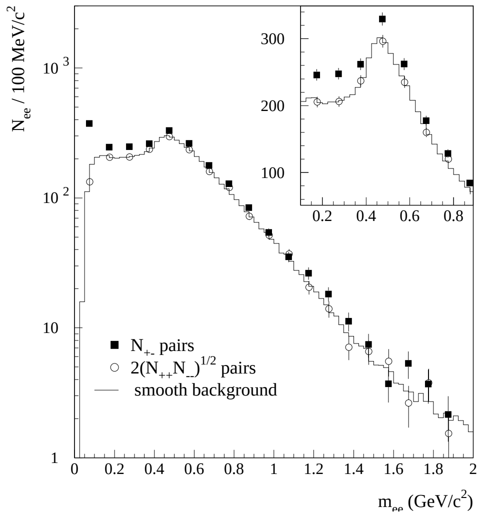

Figure 10: Raw mass spectrum of unlike-sign pairs (black squares), like-sign pairs (open circles) and smoothed background spectrum (histogram), see text. Insert shows detail on linear scale.

hits [80]; and in RICH-1 by number of photon hits or an analog sum, both signaling V tracks, see fig. 9.

CERES' main problem is background, and its first concern is to reject it without vetoing the signal. Close pairs are very harmful as the main source of combinatorial pair background. They are by far more frequent than the more massive pairs we like to study. Already a small fraction of close pairs with only *one* recognized track gives rise to random pair combinations of sufficiently large Poissonian probability to outnumber the signal. An obvious hazard is, for example, an overlooked π°-Dalitz pair with one hard electron passing the p_t^e cut; by no means a very rare event. To reject tracks lonely tracks from incomplete close pairs, certain cuts on the cleanliness of the track *environment* are imposed in RICH-1 and the silicon telescope simultaneously. The combinatorial background is drastically reduced by raising the p_t cut on single electron tracks because close pairs are soft. The combinatorial background may be estimated by counting the number of like-sign pairs, because there is no physics source. The pair signal S is obtained by subtracting the geometric mean of the like-sign contributions from the e^+e^- sample,

$$S = N_{+-} - 2\sqrt{(N_{++}N_{--}}. \qquad (6)$$

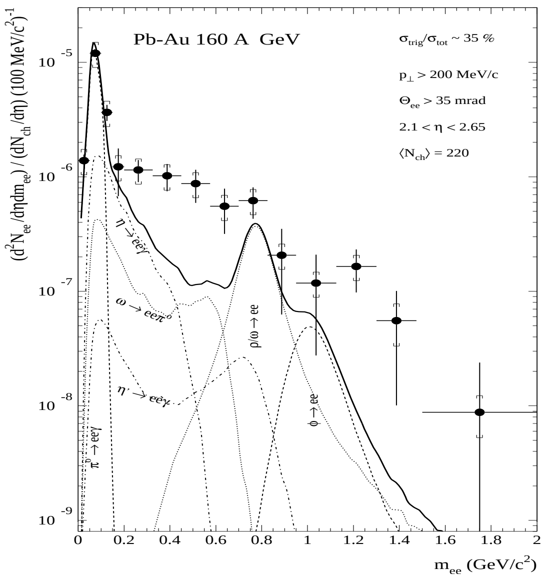

Figure 11: Invariant mass spectrum of e^+e^- pairs, data points with statistical and systematic errors (brackets). $\langle N_{ch} \rangle$=220 corresponding to the most central 35% of the geometrical cross section.

5.4 Inclusive Mass Spectra

The raw spectra of unlike-sign and like-sign pairs are shown in fig. 10. The latter spectrum was smoothed by applying an event-mixing method similar to the one used in ref [57], thus reducing statistical errors via background subtraction [77]. The structure visible in the background spectrum is due to the cut $p_t^e \leq 200$ MeV/c^2 on single electrons which depletes the spectrum below about twice the cut value. The final sample of Dalitz-type pairs, for invariant masses below 200 MeV/c^2, is 1038±55 at a signal-to-background ratio S/B= 1.05. Above 200 MeV/c^2, we find a signal of 648±105 pairs with S/B= 1/8.

The mass spectra have been corrected for pair reconstruction efficiency. For this purpose, the response of all detectors to Monte-Carlo generated signal tracks from neutral meson decays was fully simulated on GEANT[82] basis, overlaid to real data and analyzed in the standard software chain. On averaging over the triggered N_{ch} distribution, about 50% of the tracks were reconstructed, implying a pair reconstruction efficiency of about 25%. The background rejection cuts reduce the efficiency to about 12%. The efficiency decreases with increasing charged multiplicity, from 16% at N_{ch}=120 to 9% at N_{ch}= 350.

The final invariant mass spectrum is shown in fig. 11. The electron pair yield is normalized to the average charged-particle density $\langle N_{ch} \rangle$=220 measured in the spectrometer acceptance [s]. The systematic errors contain uncertainties in the background smoothing procedure, the absolute background level, the reconstruction efficiency, its N_{ch} dependence, and the determination of $\langle N_{ch} \rangle$. Adding these contributions in quadrature amounts to 25–40%, depending on mass. Systematic errors in different mass bins are strongly correlated. The data are compared to the usual hadronic cocktail of neutral-meson decays, scaled up from p–p. The improved momentum resolution has been used in the final convolution of the laboratory momenta of the simulated decay electrons.

The first four data points agree very well with the π° and η Dalitz contributions which dominate the cocktail at this part of the spectrum. Above 200 MeV/c^2, the yield is strongly enhanced, and the largest excess over the cocktail is observed around 0.5 GeV/c^2. These features are familiar already from S–Au. The enhancement factors for the full mass range (I) 0.2$\leq$ m $\leq$ 2.0 GeV/c^2, as well as for the region (II) 300$\leq$ m $\leq$ 700 MeV/c^2 are

$$(I): \; 3.5 \pm 0.4\,(stat) \pm 0.9\,(syst); \;\; (II): \; 5.8 \pm 0.8\,(stat) \pm 1.5\,(syst). \quad (7)$$

The spectrum is featureless and has little resemblance to the shape of the generator spectrum. The ρ/ω resonance peak is conspicuously absent, only the sharp fall-off towards high masses might be reminiscent of it. The mass resolution of $\sigma_m/m_{\rho/\omega} \approx 8\%$ should clearly be capable to expose the peak structure, as can be seen from the cocktail in fig. 11. In the invariant mass spectra for p–Be and p–Au, a prominent peak is seen with inferior mass resolution of only 11% at $m_{\rho/\omega}$ (fig. 2).

5.5 Stability of results

At a signal-to-background level of 1/8 one has to be concerned about how reliable and stable a signal is that results from subtracting two almost equally large numbers. Even by careful inspection of fig. 10, it would be hard to tell by their spectral shapes which is signal and which is background – at least for masses above 200 MeV/c^2. This raises doubt whether the background has been subtracted correctly.

The optimization of quality and rejection cuts was done without feedback from the signal itself, in order not to exploit statistical fluctuations likely to

[s] The mean particle density given in a preliminary account of the data at QM'96 was too high by 15% due to an overcorrection of hit pile-up [80].

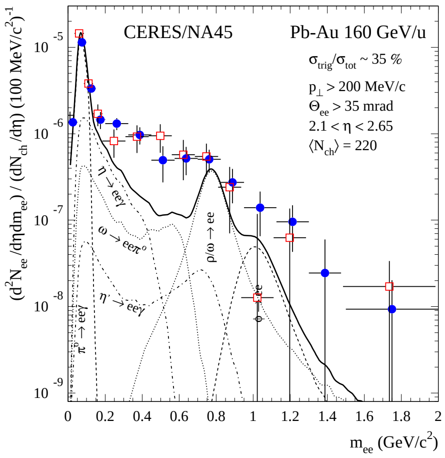

Figure 12: Invariant mass spectra of e^+e^- pairs with final background rejection cuts applied (S/B= 1/8, full circles) and without them (S/B= 1/25, open squares). See text.

occur in a finite sample. All quality cuts were optimized in Monte-Carlo simulations, and the rejection power (in lack of realistic background simulations) was judged independently from the measured like-sign pair background.

We have checked the stability of our results in two ways: (i) all rejection cuts have been varied simultaneously at random within a window of $\pm 15\%$ around the optimum values. Data analyses were performed for several hundred multidimensional sets of cut parameters. The efficiency-corrected results remained within the systematic errors quoted. (ii) The final background rejection cuts were left out so that the S/B ratio deteriorated from 1/8 to 1/25. Despite a threefold increase of the background level, the *absolute magnitude* of the signal does not show the increase to be expected would it contain a sizeable fraction of unsubtracted background, see fig. 12. That the signal remains so remarkably stable tells us that this fraction is small and within the (admittedly large) errors. The stability of the shape, however, was to be expected.

5.6 Centrality Dependence

The size of the data set allowed to investigate the multiplicity dependence of the new dilepton source. Fig. 13 compares mass spectra of semi-peripheral collisions, $\langle N_{ch} \rangle$=120, with those of central collisions of the upper 8% of σ_{geo}, $\langle N_{ch} \rangle$=350. It seems fair to state that within considerable uncertainties of the data points, the shape remains qualitatively unchanged, while the enhancement is definitely larger for central collisions.

Let us have a closer look. The pair yield integrated over the mass spectrum

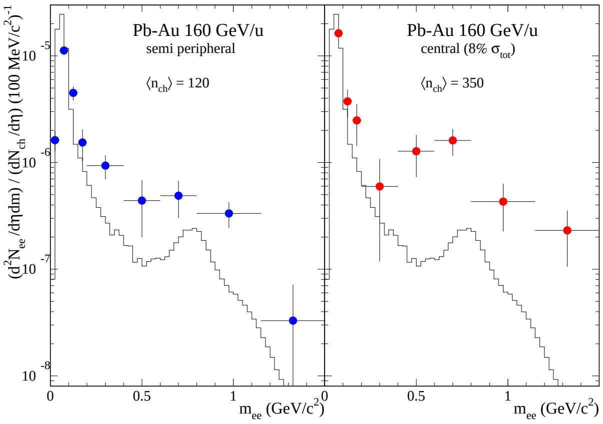

Figure 13: Preliminary invariant mass spectra of e^+e^- pairs for semi-peripheral collisions, $\langle N_{ch}\rangle$=120 (left), and central collisions, $\langle N_{ch}\rangle$=350 corresponding to the upper 8% of σ_{geo}.

from 0.2 to 2.0 GeV/c^2, and normalized to the charged particle density, is displayed in fig. 14 for four points at particle densities between 120 and 350, and two points close to zero on that scale, taken from p–Be and p–Au [57]. The quantity plotted is

$$\left(\int_{0.2}^{2.0}\left\langle\frac{dN_{ee}(m;\nu)}{d\eta}\right\rangle dm\right) / \langle\ \nu\ \rangle \quad versus \quad \nu = \frac{dN_{ch}}{d\eta}, \tag{8}$$

where edgy brackets indicate averaging over CERES acceptance. Pairs from hadron decays scale *linearly* with particle density and will give a constant ratio at the level of the horizontal line in fig. 14 which is fixed by the two p–A data points. The straight line obtained by linear regression [t] translates into a *quadratic* dependence of the e^+e^- yield in Pb–Au collisions.

The declaration of observed quadratic multiplicity dependence of the pair yield might alert suspicion, because the pair background by its combinatorial origin is bound to raise in exactly this manner. In order to assure correct background subtraction at varying event density, all procedures to optimize background rejection cuts, and the independent optimization of the signal efficiency by embedding MC events into data, were done for four different multiplicity bins spanning the entire range of triggered events. For the present discussion it may suffice to use the previous argument (ii) from sect. 5.5, where it was shown that an increase of the combinatorial background did not alter the magnitude of the extracted signal.

[t] to the four Pb–Au points only; the perfect pointing to the p–A points is fortuitous.

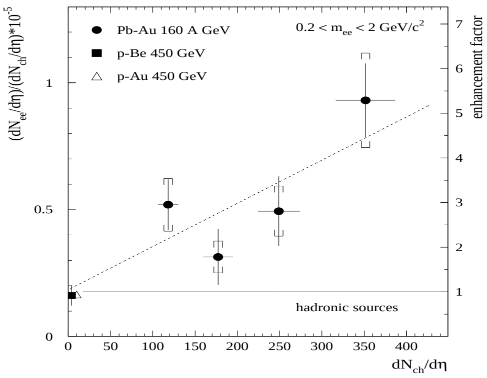

Figure 14: Normalized integral pair yield *vs* $dN_{ch}/d\eta$, see eqn. 8. For hadron decays *linear* in $dN_{ch}/d\eta$, normalized yields are *constant* and given by the p–Be, Au data points. Pb–Au data points follow in fact a regression line through the p–A points supporting a *quadratic* dependence of the pair yield.

5.7 p_t spectra

To explore the physics nature of the excess, we like to study the dependence on p_t of the *pair* [u]. The p_t cut on the tracks, $p_t^e \geq 200$ MeV/c, sharply depletes the yield both in mass and in p_t^{ee} below about twice that value. Fig. 15 shows p_t^{ee} spectra for three different intervals of invariant mass in absolute normalization. The good agreement between data and hadronic cocktail in the lowest mass bin, m≤ 200 MeV/c^2, is expected as we are looking at Dalitz decays. A striking overshoot of data at very low p_t^{ee} is seen in the mass region $0.2 \leq$ m ≤ 0.6 GeV/c^2; spectra here are visibly affected by the p_t^e cut on the track. For masses above 600 MeV/c^2, enhancement persists over the entire spectrum, although it is much more pronounced below $p_t^{ee} \leq 0.5$ MeV/c.

Let us compare mass spectra with different p_t^{ee} selection. A spectrum of low transverse pair momenta $p_t \leq 400$ MeV/c is shown in the left part of fig. 16. The gradual cut-off for m≤ 400 MeV/c^2 is trivially caused by the p_t^e cut on tracks. Now, the enhancement around 500 MeV/c^2 has grown to more than one order of magnitude! There is no indication of the vector meson peak other than that the upper edge of the broad bump which centers at m≈ 0.4 GeV/c^2 is still marked by the high-mass flank of the ρ/ω *cocktail.* Inspecting the complementary mass spectrum with $p_t^{ee} \geq 0.4$ GeV/c shown at the right hand side in the preliminary figure [v], a dramatic *reduction* in enhancement is

[u] for clarity we write sometimes p_t^e and p_t^{ee} to avoid confusion.
[v] obtained by bin-for-bin subtraction of fig. 11 and the left-hand plot of fig. 16.

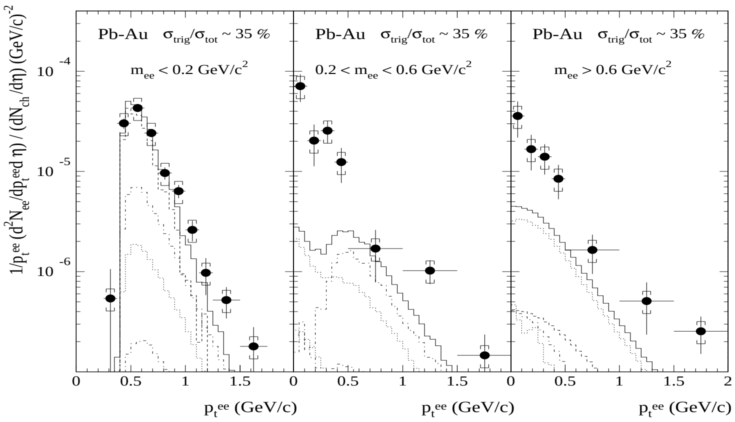

Figure 15: Lorentz-invariant p_t^{ee} distributions for three mass intervals. The hadronic cocktail is shown for comparison; its two largest components besides the total are from left to right: π^0- and η-Dalitz; η- and ω-Dalitz; and direct decays of ρ/ω and ϕ, respectively.

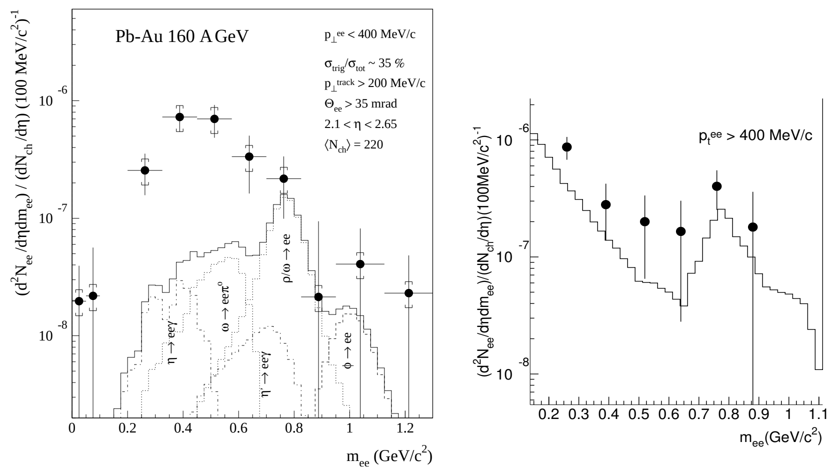

Figure 16: Invariant mass spectrum of e^+e^- pairs with small transverse momentum $p_t^{ee} \leq 400$ MeV/c (left), and complement with $p_t^{ee} \geq 400$ MeV/c (right), with respective hadronic cocktails. Preliminary.

obvious, while the resonance peak seems to reappear. This suits the fact that ρ/ω is prominently visible in the hard muon pair spectra of NA38/50, where the low-mass enhancement, as we have seen, appears to be very moderate.

5.8 Medium modifications empirical

The comparison of the S–Au and S–W dilepton data with so many different model calculations in sect.4 strongly suggested that in-medium modifications of vector mesons are essential ingredients for a description of low-mass dilepton spectra. Two scenarios remained as competing choices, those which incorporate falling vector-meson masses, and those which change the propagation of vector mesons due to collisions. In fig. 17, the calculation of Rapp, Chanfray, Wambach [74] is shown together with CERES data for central Pb–Au collisions [80] to demonstrate that the spectral function approach describes the data also quite well. In the continuation of this work, the p-wave ρN scattering was implanted into the transport approach of Cassing, and very good agreement with CERES and HELIOS/3 data is obtained [75].

At present data accuracy no empirical handle is in sight to differentiate between the two secenarios of medium modifications, especially as the deviations between protagonists have become more subtle and tend to hide within the large data errors. It is of little use therefore to reiterate a detailed comparison. Instead, it might be worthwile to state a few common trends which become plain by looking over the calculations that address CERES Pb–Au data.

Let us first repeat the characteristic of the data which is seen unchanged from S–Au collisions. The spectra are *featureless*, show no resonance peak (the right-hand spectrum of fig. 16 discussed below is the only exception). For

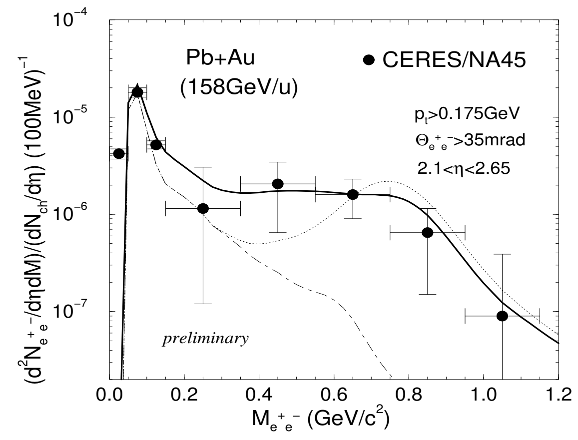

Figure 17: e^+e^- spectrum for Pb–Au central, calculated by Rapp et al. [74] compared to CERES data [80]. Neutral meson decays with free ρ propagator (dotted line), with in-medium ρ propagator (full curve), and Dalitz decays shown separately (dashed-dotted line).

semi-central collisions, above ≈ 0.2 GeV/c^2 the yield gently slopes down with mass or forms a plateau until the ρ/ω position, from where on it falls off more steeply (fig. 11); from m$\approx$ 0.3 GeV/c^2 to the ρ/ω position it decreases by a factor of about 2. For central collisions, a broad mountain ridge forms with its highest elevation between 0.4 and 0.6 GeV/c^2 (fig. 13) [w].

The calculations available [x] display the following trends clearly: spectra with *free* masses or *free* spectral functions have a local *minimum* around 0.3-0.4 GeV/c^2 from which they raise by a factor of 1.5 to 2.5 to a prominent *ρ/ω peak.* 'Free' shapes are therefore 'orthogonal' to the experimental shape, maxima and minima are at exchanged positions, that is why they cannot describe the data.

In pragmatic terms, all spectra with medium modifications are closer to the experimental shapes than their 'free' counterparts, with the tendency to fill the minimum and smear out the resonance peak. It works very well for (7)- falling masses, (8)- full spectral function, (1)- falling masses, (2)- full spectral function; pretty well for (5)- falling mass (scenario D); it does not work for (6) and (9), although the latter approach is very similar to (2) and (8) as remarked recently [23]. It seems that pion annihilation in the mass around 0.4 GeV/c^2 is similarly amplified by a broadened full spectral function as by a shifting pole, so that both types of theories describe the data well. It was proposed [75] that broadening without mass shift of the rho might reveal itself in the high mass tail between ρ and ϕ; future data with improved statistics, but low p$_t$, might be able to distinguish the in-medium processes this way, but secondary processes in this mass region [38] have to be accounted for.

Last not least, I like to discuss and put into possibly useful perspective the transverse momentum dependence. We have observed an extraordinary strong sensitivity of the mass spectrum of fig. 11 when pair transverse momenta *below* or *above* 400 GeV/c were selected. No dependence nearly as strong [y] was to be expected from calculated dilepton p$_t$ distributions which have almost identical slopes for 'free' and 'full' spectral functions [83,75].

The low p$_t^{ee}$ spectrum looks as Nature had medium modifications grossly overdone (fig. 16 right). Selecting p$_t^{ee} \geq 0.4$ GeV/c, quite to the contrary, the spectrum has almost reached the canonical shape of a 'free' rho-meson calcu-

[w] The preliminary spectra presented at QM'96 are within errors fully consistent with the final ones shown here and comply with the characteristic just given. It therefore does not matter that all model comparisons were done with preliminary data.

[x] These are in alphabetic order: (1) Bratskovskaya, Cassing [83]; (2) Cassing, Bratkovskaya, Rapp, Wambach [75]; (3) Filip, Pisut [84]; (4) Huovinen, Ruuskanen, Sollfrank [90]; (5) Hung, Shuryak (fig.4d) [68]; (6) Koch, Song [69]; (7) Li, Ko, Brown, Sorge [66]; (8) Rapp, Chanfray, Wambach [74]; (9) Steele, Yamagishi, Zahed [51]; (10) Winckelmann et al. [72].

[y] as expressed e.g. by the double-ratio of the yield at m=m$_\rho$ to the yield at m= 0.5 GeV/c, comparing the two p_t selections.

lation! From which I like to suggest that medium modifications of the dilepton producing processes are much sharper localized at low p_t than described up to now, and pretty distinct from the p_t range of processes producing primary ρ and ω. Recalling that NA38/50 has a considerably higher p_t cut at low masses, we may stop to wonder about the small low-mass enhancement observed, on one side, and the prominent exposure of the ρ/ω on the other, features that go hand in hand. A proper description of the p_t dependent spectral shapes is obviously called for, and it might even help to distinguish the in-medium physics alternatives. If established, the strong p_t dependence is of practical advantage for precision resolution studies of the ω strength that CERES is preparing for: too strong medium modification covering the ω resonance and thus impeding a high resolution measurement could be controlled by raising the p_t^{ee} cut by no more than a few hundred MeV/c.

6 Summary and Outlook

In summary, the enhancement observed in low-mass dilepton spectra is corroborated with recent CERES data from Pb–Au collisions. The data also suggest a quadratic dependence of the pair yield on charged-particle density which is in support of pion annihilation as the dominant hadro-chemical reaction in hot and dense environment that produces low-mass dileptons. There is overwhelming evidence, however, that in order to describe CERES and HELIOS/3 low-mass data, medium modifications of the mediating vector meson, the rho meson in the first place, have to be included. It will be a big challenge for future experiments to discriminate the falling-mass scenario as a precursor of chiral symmetry restoration, from a more conventional broadening by collisions. The processes affected most by medium modifications seem to be sharply located at low transverse pair momentum which is presently not thoroughly understood. To gain new insights, coming CERES experiments with a spectrometer upgraded by a large TPC for much better mass resolution [95] will try to do precision spectroscopy of the more long-lived vector meson resonances ω and ϕ and study also the dependence of medium modifications on baryon density, at reduced SPS energy. The NA50 program improved with pixel detectors for better rejection of background and improved acceptance at low p_t will hopefully take up the challenge.

Acknowledgments

It is a pleasure to acknowledge fruitful discussions with G.E. Brown, W. Cassing, B. Friman, L. Kluberg, C.M. Ko, V. Koch, G.Q. Li, C. Lourenco, H.J. Pirner and J. Wambach, and with my colleagues from CERES, especially A.

Drees. We are grateful for support from the German-Israeli Foundation for Scientific Research under Contract I-366-194.07. I

References

1. See for up-to-date general review: J.W. Harris and B. Müller, *Ann. Rev. Nucl. Part. Sci.* **46**, 71 (1996); Proceedings of Quark Matter Conferences 1996 in Heidelberg, *Nucl. Phys.* A **610**, (1996), and 1997 in Tsukuba, to appear in *Nucl. Phys.* A.
2. J. Hüfner, S.P. Klevansky, P. Rehberg, *Nucl. Phys.* A **606**, 260 (1996)
3. P. Braun-Munzinger, J. Stachel, J.P. Wessels and N. Xu, *Phys. Lett.* B **365**, 1 (1996).
4. E. Shuryak and T. Schäfer, *Ann. Rev. Nucl. Part. Sci.* **47**, 359 (1997); G.E. Brown and M. Rho, *Phys. Rep.* 269, 333 (1996); W. Weise, *Nucl. Phys.* A **610**, 35c (1996).
5. R. Pisarski, *Phys. Lett.* B **110**, 155 (1982).
6. K. Haglin, *Nucl. Phys.* A **584**, 719 (1995)
7. G.E. Brown and M. Rho, *Phys. Rev. Lett.* **66**, 2720 (1991). See also G.E. Brown, M. Buballa and M. Rho, *Nucl. Phys.* A **609**, 519 (1996).
8. T. Hatsuda and S.H. Lee, *Phys. Rev.* C **46**, R34 (1992). 30
9. B. Friman and M. Rho, *Nucl. Phys.* A **606**, 303 (1996).
10. R.D. Pisarski, *Phys. Rev.* D **52**, R3773 (1995).
11. J. Kapusta and E.V. Shuryak, *Phys. Rev.* D **49**, 4694 (1994).
12. M. Masera (HELIOS/3 Coll.), *Nucl. Phys.* A **590**, 94c (1995).
13. G. Agakichiev et al., *Phys. Rev. Lett.* **75**, 1272 (1995).
14. M. Gonin et al. (NA50 Collab.), *Nucl. Phys.* A **610**, 404c (1996); C. Lourenço, *loc. cit.*, 552c.
15. C. Lourenço et al. (NA38 Collab.), *Nucl. Phys.* A **566**, 77c (1994); C. Lourenço (NA38 Collab.), *Proc. Intern. Workshop XXIII on Gross Properties of Nuclei and Nuclear Excitations*, Hirschegg 1995; C. Lourenço, Doctoral Thesis, Univeridade Tecnica de Lisboa (1995).
16. J.P. Wurm et al. (CERES Coll.), *Nucl. Phys.* A **590**, 103c (1995);
17. G.Q. Li, C.M. Ko, G.E. Brown, *Phys. Rev. Lett.* **75**, 4007 (1995).
18. G. Chanfray, R. Rapp and J. Wambach, *Phys. Rev. Lett.* **76**, 368 (1996);
19. CEBAF Experiment E94-002, P.Y. Bertin, M. Kossov, B.M. Preedom
20. G.J. Lolos et al., *Phys. Rev. Lett.* **80**, 241 (1998).
21. W. Schön, H. Bokemeyer, W. König, V. Metag (HADES Collaboration) GSI Letter of Intent.
22. A. Drees, *Nucl. Phys.* A **610**, 536c (1996); Proceedings of the Intl. Workshop XXV on Gross Properties of Nuclei and Nuclear Excitations,

Hirschegg 1997, eds. H. Feldmeier et al., GSI Darmstadt 1997; Preprint Gatlinburg Conference 1977
23. I. Tserruya, *Nucl. Phys.* A **590**, 127c (1995); Proc. Quark Matter 97.
24. R. Vogt, B. Jacak, P.L.M. Gaughey, and P.V Ruuskanen, *Nucl. Phys.* A **583**, 693 (1995);
25. S. Gavin et al., *Phys. Rev.* C **54**, 2606 (1996).
26. P. Braun-Munzinger, D. Miskowiec, A. Drees, C. Lourenço, *Eur. Phys. J.* C **1**, 123 (1998).
27. T. Sjostrand,*Comp. Phys. Comm.* **82**, 74 (1994). 29
28. M.C. Abreu et al. (NA50 Collab.), *Phys. Lett.* B **410**, 337 (1997); L. Ramello et al. (NA50 Coll.), Proceed. Quark Matter 1997.
29. T. Matsui and H. Satz, *Phys. Lett.* B **178**, 416 (1986)
30. J.-P. Blaizot and J.-Y. Ollitraut, *Nucl. Phys.* A **610**, 452c (1996); D. Kharzeev, M. Nardi and H. Satz, hep/9707308.
31. C. Spieles et al., LBNL-40497.
32. H. Sorge, H. Stöcker, W. Greiner, *Ann. Phys.* **192**, 266 (1989); S.A. Bass et al., nucl-th/9703035
33. E. Shuryak, *Phys. Rev.* C **55**, 961 (1997).
34. J. Cleymans, V.V. Golovizin, K. Redlich, *Z. Phys.* C **59**, 495 (1993); P. Lichard, *Phys. Rev.* D **51**, 6017 (1995); H.C. Eggers et al., *Phys. Rev.* D **53**, 4822 (1996)
35. E.V. Shuryak, *Phys. Lett.* B **78**, 150 (1978).
36. L.D. McLerran and T. Toimela, *Phys. Rev.* D **31**, 545 (1985).
37. Ch. Gale and P. Lichard, *Phys. Rev.* D **49**, 3338 (1994); Ch. Song, C.M. Ko, and Ch. Gale, *Phys. Rev.* D **50**, R1827 (1994); S. Gao and Ch. Gale, *Phys. Rev.* C **57**, 254 (1998); A.V. Leonidov and P.V. Ruuskanen, hep-ph/9709343 1997.
38. G.Q. Li, G.E. Brown, C. Gale, C.M. Ko, these proceedings.
39. K. Kajantje, J. Kapusta, L. McLerran, A. Mekjian, *Phys. Rev.* D **34**, 2746 (1986); C. Gale and J. Kapusta, *Phys. Rev.* C **35**, 2107 (1987); J. Cleymans, K. Redlich, and H. Satz, *Z. Phys.* C **52**, 517 (1991); P. Koch, *Z. Phys.* C **57**, 283 (1993); B. Kämpfer, P. Koch, and O. Pavlenko, *Phys. Rev.* C **49**, 1132 (1994).
40. G. Roche et al., *Phys. Rev. Lett.* **61**, 1069 (1988); C. Naudet et al., *Phys. Rev. Lett.* **62**, 2652 (1988);
41. L.M. Barkov et al., *Nucl. Phys.* B **256**, 365 (1985).
42. H.B. O'Connell, B.C. Pearce, A.W. Thomas and A.G. Williams, *Progr. Part. Nucl. Phys.* 39, 201 (1997).
43. C.M. Ko and G.Q. Li, *J. Phys.* G **22**, 1673 (1994); G.Q. Li and C.M. Ko, *Nucl. Phys.* A **582**, 731 (1995).

44. C.L. Korpa and S. Pratt, *Phys. Rev. Lett.* **64**, 1502 (1990).
45. Ch. Song and V. Koch, *Phys. Rev.* C **54**, 3218 (1996).
46. M. Herrmann, B.L. Friman, W. Nörenberg, *Nucl. Phys.* A **545**, 267c (1992); *Nucl. Phys.* A **560**, 411 (1993).
47. M. Asakawa, C.M. Ko, P. Levai and X.J. Qiu, *Phys. Rev.* C **46**, R1159 (1992).
48. G. Chanfray and P. Schuck, *Nucl. Phys.* A **545**, 271c (1992); *Nucl. Phys.* A **555**, 329 (1993);
49. B. Friman and H.J. Pirner, *Nucl. Phys.* A **617**, 496 (1997).
50. G. Chanfray, R. Rapp and J. Wambach, *Phys. Rev. Lett.* **76**, 368 (1996); R. Rapp, G. Chanfray and J. Wambach, *Nucl. Phys.* A **617**, 472 (1997).
51. J.V. Steele, H. Yamagishi and I. Zahed, *Phys. Lett.* B **384**, 255 (1996); *Phys. Rev.* D **56**, 5605 (1997); hep-ph/9802256
52. B. Friman, these proceedings.
53. I. Zahed, these proceedings.
54. M. Dey, V.L. Eletsky, and B.L. Ioffe, *Phys. Lett.* B **252**, 620 (1990).
55. R.C. Hwa and K. Kajantje, *Phys. Rev.* D **32**, 1109 (1985)
56. R.J. Porter *Phys. Rev. Lett.* **79**, 1229 (1997).
57. G. Agakichiev et al. (CERES/TAPS Collab.), Neutral meson production in p-Be and p-Au collisions at 450 GeV beam energy; G. Agakichiev et al. (CERES/TAPS Collab.), Systematic study of low-mass electron pair production in p-Be and p-Au collisions at 450 GeV/c, Eur. Phys. J. C, in press;
58. A. de Falco and C. Lourenço, Internal paper, CERN 1997
59. E. Scomparin et al. (NA50 Collab.), *Nucl. Phys.* A **610**, 331c (1996).
60. A. de Falco (for NA38/50 Collaboration), Proceedings Quark Matter '97.
61. M.C. Abreu et al. (NA50), Addendum to Proposal SPSLC/P265, CERN/SPSC 97-22
62. M.C. Abreu et al. (NA38 Collab.), *Phys. Lett.* B **368**, 239 (1996); D. Jouan for NA38/50, Preprint IPN Orsay 1997; Proceedings Quark Matter 1997.
63. W. Ehehalt and W. Cassing, *Nucl. Phys.* A **602**, 449 (1996).
64. H.J. Schulze and D. Blaschke, *Phys. Lett.* B **386**, 429 (1996).
65. W. Cassing, W. Ehehalt, and C.M. Ko, *Phys. Lett.* B **363**, 35 (1995).
66. G.Q. Li, C.M. Ko, G.E. Brown, *Nucl. Phys.* A **606**, 568 (1996); G.Q. Li, C.M. Ko, G.E. Brown, H. Sorge, *Nucl. Phys.* A **611**, 539 (1996).
67. D.K. Srivastava, B. Sinha, and Ch. Gale, *Phys. Rev.* C **53**, R567 (1996).
68. C.M. Hung and E.V. Shuryak, *Phys. Rev.* C **56**, 453 (1997).
69. V. Koch and Ch. Song *Phys. Rev.* C **54**, 1903 (1996).
70. R. Baier, M. Dirks, and K. Redlich, *Phys. Rev.* D **55**, 4344 (1997).

71. J. Murray, W. Bauer, and K. Haglin, *Phys. Rev.* C **57**, 882 (1998).
72. L.A. Winckelmann et al., *Nucl. Phys.* A **610**, 116c (1996).
73. W. Cassing, W. Ehehalt, and I. Králik, *Phys. Lett.* B **377**, 5 (1996).
74. R. Rapp, G. Chanfray and J. Wambach, *Nucl. Phys.* A **617**, 472 (1997); Proceedings of the Intl. Workshop XXV on Gross Properties of Nuclei and Nuclear Excitations, Hirschegg 1997, eds. H. Feldmeier et al., GSI Darmstadt 1997;
75. W. Cassing, E.L. Bratskovskaya, R. Rapp and J. Wambach, *Phys. Rev.* C **57**, 916 (1998)
76. G. Agakichiev et al., Low-mass e^+e^--pair production in 160 A GeV Pb-Au collisions at the CERN SPS, its dependence on multiplicity and transverse momentum, *Phys. Lett.* B, in print.
77. C. Voigt, Doctoral Thesis, University of Heidelberg, 1998; B. Lenkeit, Doctoral Thesis, University of Heidelberg, in preparation.
78. I. Ravinovich et al. (CERES Coll.), Proceedings of Quark Matter '97.
79. CERES/NA45 Report to Cogne 1995, CERN/SPSLC 95-20.
80. T. Ullrich et al., *Nucl. Phys.* A **610**, 317c (1996);
81. F. Ceretto, Doctoral Thesis, University of Heidelberg, 1998.
82. R. Brun et al., CERN DD/EE/84-1 (1984), unpublished
83. E.L. Bratskovskaya and W. Cassing, *Nucl. Phys.* A **619**, 413 (1997)
84. P. Filip and J. Pisut, *Phys. Lett.* B **411**, 187 (1997).
85. J. Sollfrank, P. Huovinen, M. Kataja, P.V. Ruuskanen, M. Prakash and R. Venugopalan, *Phys. Rev.* C **55**, 392 (1997).
86. J. Cleymans, K. Redlich, and D.K. Srivastava, nucl-th/9702004
87. R. Rapp, M. Urban, M. Buballa, J. Wambach, *Phys. Lett.* B **417**, 1 (1998)
88. C.M. Ko, V. Koch, G. Li, *Ann. Rev. Nucl. Part. Sci.* **47**, 505 (1997)
89. V. Cerny, P. Lichard, and J. Pisut, *Z. Phys.* C **31**, 163 (1986).
90. P.V. Ruuskanen, Proceedings Quark Matter 1997, P. Huovinen, P.V. Ruuskanen, J. Sollfrank, nucl-th/9803006
91. A.L.S. Angelis et al. (HELIOS/3 Collab.), CERN-PPE/97-117.
92. M.C. Abreu et al. (NA38 Collab.), *Phys. Lett.* B **368**, 230 (1996). C. Baglin et al. (NA38 Collab.), *Phys. Lett.* B **270**, 105 (1991).
93. C.M. Abreu et al. (NA50 Collab.), *Phys. Lett.* B **410**, 327 (1997).
94. R. Baur et al. (CERES Collab.), *Nucl. Instrum. Methods* A **343**, 87 (1994).
95. CERN SPSLC/P280 (CERES Collab.), Spokesperson J. Stachel